# Intracerebroventricular delivery of glatiramer acetate: a proof-of-concept treatment for Alzheimer's disease by promoting innate phagocytosis and antagonizing amyloid-β toxicity

**Xin Huang**
The Florey Institute of Neuroscience and Mental Health
**Feng Chen**
The Florey Institute of Neuroscience and Mental Health
**Larissa Doughty**
The University of Melbourne Bio21 Molecular Science and Biotechnology Institute
**Qiao-Xin Li**
The Florey Institute of Neuroscience and Mental Health
**Wensi Ou**
The Florey Institute of Neuroscience and Mental Health
**Yihan Li**
The Florey Institute of Neuroscience and Mental Health
**Candace Drysdale**
The Florey Institute of Neuroscience and Mental Health
**Arwa Alrehaili**
The Florey Institute of Neuroscience and Mental Health
**Ian E. Birchall**
The Florey Institute of Neuroscience and Mental Health
**Joelyn Wong**
The Florey Institute of Neuroscience and Mental Health
**Keunha Park**
The Florey Institute of Neuroscience and Mental Health
**Michael Lim**
The Florey Institute of Neuroscience and Mental Health
**Mujun Sun**
Monash University Department of Medicine Alfred Hospital: Monash University Central Clinical School
**Bridgette D. Semple**
Monash University Department of Medicine Alfred Hospital: Monash University Central Clinical School
**Sandy R. Shultz**
Monash University Department of Medicine Alfred Hospital: Monash University Central Clinical School

**Paul A. Adlard**
The Florey Institute of Neuroscience and Mental Health
**Michael W. Parker**
The University of Melbourne Bio21 Molecular Science and Biotechnology Institute
**Michael McKinley**
The Florey Institute of Neuroscience and Mental Health
**Colin L. Masters**
The Florey Institute of Neuroscience and Mental Health
**James S. Wiley**
The Florey Institute of Neuroscience and Mental Health
**Ben J Gu** ( ben.gu@florey.edu.au )
The University of Melbourne https://orcid.org/0000-0001-5500-4453

---

**Research article**

**Keywords:** Glatiramer acetate, Alzheimer's disease, Innate phagocytosis, Intracerebroventricular drug delivery, Long-term potentiation in the hippocampus, Cognitive function

**Posted Date:** April 11th, 2022

**DOI:** https://doi.org/10.21203/rs.3.rs-1524708/v1



---

# Abstract

**Background:** We and others have reported that glatiramer acetate promotes innate phagocytosis.

**Methods:** In this study, we investigated the interaction between glatiramer acetate and amyloid-β (Aβ) by using circular dichroism and microscale thermophoresis. Glatiramer acetate was delivered intracerebroventricularly to 22-month-old APP/PS1 mice by using mini-osmotic pumps. Mice underwent behavioural testing for two consecutive weeks after three-weeks treatment. Five weeks after implantation, animals were sacrificed and brain samples were collected for electrophysiology, immunochemistry and histopathology studies. Intracerebroventricular delivery of glatiramer acetate to sheep was also examined.

**Results:** Glatiramer acetate binds to amyloid-β within high affinity and antagonize its toxicity. Glatiramer acetate treatment significantly improved cognitive function, restored long-term potentiation, reduced soluble amyloid-β and amyloid-β plaques in aged APP/PS1 mice, and promoted energy metabolism in sheep.

**Conclusions:** Our results suggest a novel treatment strategy that targets both innate phagocytosis and amyloid-β, which may prove useful for treatment of all stages of Alzheimer's disease.


# Background

Alzheimer's disease remains incurable, despite the enormous endeavor directed at pathogenesis, diagnosis and treatment. Aβ has historically been the major therapeutic target for treatment; however, most of the clinical trials have not met their primary objectives. Multiple clinical trials have tested passive immunization against Aβ as therapy; however, only a limited proportion is able to pass through the BBB to reach the CNS. Solanezumab, targeting the central domain of Aβ, seems to have little effect on brain Aβ burden (1); only those N-terminal targeting antibodies with higher amyloid-related imaging abnormalities (ARIA) such as bapineuzumab (ARIA:15.3%) (2) and aducanumab (ARIA:13–47%, dose dependent) (3), demonstrated effective prevention of brain Aβ accumulation (2) or even reduction of Aβ burden (3). Thus, besides the antigen epitopes, it is critical for drugs targeting Aβ to access the CNS.

Glatiramer acetate (GA) is a randomly synthesized peptide polymer with four amino acids: glutamic acid, lysine, alanine and tyrosine, which is widely used to treat relapsing forms of multiple sclerosis. Several groups have reported the beneficial effects of GA in different mouse models of AD (4–7), in which GA was used as an immune stimulant and administered via the periphery. We have shown that innate phagocytosis by peripheral monocytes is defective in AD and AMD, and GA can restore phagocytic function *in vitro* (8, 9). In the current study, we employed the route of intraventricular administration of GA to avoid the blood-brain barrier and examined if it can promote Aβ phagocytosis by microglia and improve cognitive function in an AD mouse model.

# Methods

**Materials -** GA (Copaxone®, 20 mg/mL) was acquired from Teva Pharmaceuticals (average molecular weight of 6.5 KD). HiLyte Fluor488 labelled $A\beta_{1-42}$ was acquired from AnaSpec, Inc. Monoclonal antibody W0-2 ($IgG_{2a,k}$), which can specifically recognize Aβ N-terminal residues 5–8 region (10), was kindly provided by Dr. Qiaoxin Li. Alexa Fluor® 488 conjugated goat anti-mouse $IgG_{2a}$ secondary antibody was acquired from Thermo Fisher Scientific Australia. Auto-fluorescence control, isotype control, PerCP-conjugated anti-human CD45 antibody and APC conjugated anti-human CD14 antibody were purchased from BD Biosciences ANZ. RPE conjugated anti-human CD16 antibody was purchased from DAKO® Agilent Technologies Australia Pty Ltd.

# Real time in vitro phagocytosis of beads assay

Human PBMCs ($2 \times 10^6$/mL) were resuspended in 100 µL Hepes-buffered Na medium (145 mM NaCl, 5 mM KCl, 10 mM Hepes, 0.1% bovine serum album, 5 mM glucose, 0.1 mM $CaCl_2$ and pH = 7.50). Cells were labelled with APC conjugated anti-human CD14 mAb at 4°C for 15 min. After staining, cells were washed once with Na medium and then resuspended in 1.0 mL Na medium. The phagocytosis assay was performed as previously described (8, 9). Briefly, all samples were kept at 37°C with constant stirring using a Time Zero module (Cytek Development Inc.). Cells were pre-incubated with 100 µg/mL CPX for 10 min or with 20 µM Cytochalasin D (Sigma-Aldrich, St Louis, MO) for 20 min at 37°C prior to the addition of 1.0 µm YG beads (Polysciences, Inc.). Cytochalasin D is a cell permeable fungal toxin that disrupts actin polymerization and inhibits phagocytosis, which is used to show non-specific binding by cells. The beads uptake was captured by a FACSCalibur flow cytometer (BD Bioscience). The linear mean channel of fluorescence intensity for each gated subpopulation over successive 10 s intervals was analysed by WinMDI software (version 2.9, by Joseph Trotter, The Scripps Research Institute, La Jolla, CA) and plotted against time. The beads uptake curve in the first 6 min was analysed. Fresh C57BL/6 mouse PBMCs (pooled blood from multiple animals) were labelled with APC conjugated anti-mouse CD11b mAb. The rest procedures are the same as above.

**Microscale thermophoresis (MST)** – MST was used to determine the interaction between GA and $A\beta_{1-42}$. In brief, HiLyte Fluor488 labelled $A\beta_{1-42}$ (80 nM, in PBS) was mixed 1:1 (volume) with serially diluted GA. Measurements were performed in standard treated capillaries on a Monolith NT.115 system using 95% LED and 40% IR-laser power. The IR-Laser was used to create a localized microscopic temperature gradient in the capillary. Simultaneously, local changes of fluorescence intensity due to the motion of Aβ in the glass capillaries were detected. The signal was recorded for IR-laser on and off stages with varying concentration of the GA. Changes of the thermophoretic property were observed as changes in fluorescence intensity.

**Circular dichroism (CD) spectroscopy** – CD is a useful technique for studying changes in the protein structure and protein–protein interactions in solution. CD in the far ultraviolet region (178–260 nm) arises from the amides of the protein backbone and is sensitive to the conformation of the protein. Molar ellipticity was acquired for $A\beta_{1-42}$ alone, GA alone and mixture of both. Binding constants were

determined by titration of Aβ by GA. Varied degrees of temperature on protein denaturation were employed to determine binding constants as well.

**Western blotting –** Samples containing Aβ and GA were mixed with loading buffer and reducing agent (DTT, 50 μM), followed by heating at 95 $^{o}$C for 5 minutes. The mixtures were loaded to a 10-well pre-casted mini gel (NuPage). Electrophoresis was running with MES buffer at 100V for 50 minutes. Proteins were transferred to nitrocellulose membrane at 100V for 35 minutes. Immunodetection was performed using anti-Aβ antibody (clone W0-2) (10).

**Aβ absorption on monocyte –** Anti-coagulant human peripheral blood was treated for 15 minutes at 37°C with one of following treatments: 2.2 μM $A\beta_{1-42}$ alone, 22 μM GA alone, or a mixture of both. After incubation, blood cells were washed twice, and red cells were lysed. Cells were stained with anti-Aβ mAb (clone W0-2) and the FITC conjugated secondary antibody, followed by extensive wash and CD14 and CD16 staining. Cells were analysed by flow cytometry.

**Cell surface Aβ staining** – Anti-Aβ antibody (clone W0-2) (20 μg/mL) was added into 100 μL whole blood. After a 15-min incubation at room temperature with gentle rocking, blood samples were washed twice with phosphate buffer and Alexa Fluor® 488 conjugated goat anti-mouse $IgG_{2a}$ secondary antibody was added at a final concentration of 15 μg/mL. After another 15-min incubation, red blood cells were lysed for 10 min using BD FACS Lysing Solution. Cells were then washed once with phosphate buffer and resuspended in 0.5 mL phosphate buffer. For further characterization of the positive cell populations, cells were washed again and stained with PE conjugated anti-human CD16 antibody, PerCP-conjugated anti-human CD45 antibody and APC conjugated anti-human CD14 antibody. Cells were washed and resuspended for FACS again. A tube of secondary antibody alone was used as control. All samples were tested together with an auto-fluorescence control, an isotype control and a secondary antibody alone control.

**MTT cytotoxicity assay –** SH-SY5Y cells were cultured in DMEM medium with 10% fetal bovine serum (FBS), 50 units/mL penicillin and 50 μg/mL streptomycin to full confluence. Cells (~ 10,000 in 100 μL) were then seeded to a 96-well plate and cultured for 48 hours. Media were discarded and replace by with 100 μL of Opti-MEM reduced serum medium free of phenol red or serum. $A\beta_{1-42}$ (10 μM) was added to duplicate wells with escalating amount of GA by molar ratios: 1:0, 1:0.1, 1:0.5, 1:1, 1:3 and1:7. Vehicle and GA alone (10 μM) were used as controls. After 4 hours incubation, 10 μL of MTT (stock concentration of 12 mM) was added to culture media. A negative control was set using 10 μL of the MTT stock solution added to 100 μL of medium alone. Cells were then incubated at 37°C for another 4 hours. MTT formazan was dissolved in 50 μL DMSO and the absorbance was read at 540 nM.

**Multi-electrode array (MEA) electrophysiology on LTP –** An acute effect of GA on Aβ-induced LTP impairment in brain slices from naïve C57/BL mice and a chronic effect of GA on LTP in brain slices from 22-month old APP/PS1 mice with or without 28- day intracerebroventricular administration of GA were investigated. The procedure of recording LTP by MEA was described in previous studies (11, 12). Briefly,

mice (C57BL/6J, aged from 12 to 15 weeks old or APP/PS1, aged 22-month-old after a 4-week treatment (icv) with or without GA), were anaesthetised with isoflurane and decapitated. Whole brains were quickly removed and place in ice-cold, oxygenated (95% $O_2$, 5% $CO_2$) cutting solution (composition in mmol·$L^{-1}$: 206 sucrose, 3 KCl, 0.5 $CaCl_2$, 6 $MgCl_2$–$H_2O$, 1.25 $NaH_2PO_4$, 25 $NaHCO_3$, and 10.6 D-glucose). A transverse hippocampal slice (350 μm) was prepared with a VT 1200S tissue slicer (Leica) and quickly transferred to 34°C artificial CSF (aCSF; composition in mmol·$L^{-1}$: 126 NaCl, 2.5 KCl, 2.4 $CaCl_2$, 1.3 6 $MgCl_2$–$H_2O$, 1.25 $NaH_2PO_4$, 25 $NaHCO_3$, and 10 D-glucose) for 30 min. After further recovery of 1-hr equilibrium in oxygenated aCSF at room temperature, the slices were transferred to a submersion recording chamber. An acute hippocampal slice was mounted on a MEA chip composed of 60 titanium electrodes (30-μm diameter) spaced 200 μm apart (60MEA200/30iR-Ti: MCS GnbH, Reutlingen, Germany). The slice was immobilized using a harp slice grid (ALA Scientific Instruments, New York, USA). The slice was continuously perfused with carbonated aCSF (3 ml·$min^{-1}$ at 32°C) during the whole recording session. Recordings were collected from the layer of stratus radiatum in CA1 as a major targeted dendritic synaptic site of Schaffer collateral projections from the CA1/CA3. Schaffer collaterals at CA1/CA3 were stimulated by injecting a biphasic current waveform (100 μs) through one selected electrode at 0.033 Hz. Care was taken to place the stimulating electrode in the same region from one slice to the other. Following a 20-min incubation period, slices were continuously stimulated with medium-strength stimuli. When stable evoked fEPSPs were detected (for at least 20 min), the stimulus threshold was determined. After recording at least 30 min of stable baseline of EPSPs, LTP was induced by applying three bursts of high frequency stimulus (HFS; 3 × 100 Hz, 500 ms width with 20-s intertrain interval) at the tested stimulation intensity and then fEPSPs were further recorded for another 30 min. Administration of an agent (either Aβ or copaxone or a mixture of both) was executed by 5 min' (the 18th to 22nd min) perfusion of agent-contained aCSF. The peak-to-peak amplitude of field EPSPs (fEPSPs) was analyzed by using LTP-Analyzer (MCS GmbH, Reutlingen, Germany). LTP was expressed as the percentage increase of fEPSP 2 min after HFS (high frequency stimulation) over the baseline fEPSP.

# Membrane fluidity test

Anti-coagulated peripheral blood (200 μL) was stained with PerCP-conjugated anti human CD14 and RPE-conjugated anti human CD16 for monocytes and incubated for 10 min at room temperature in the dark. The samples were then labelled with 5 μM of lipophilic probe TMA-DPH for 5 mins at 37°C. Following this, the samples were treated with 5 μM of $A\beta_{1-42}$, 100 μg/mL of GA alone or 5 μM of $A\beta_{1-42}$ and 100 μg/mL of GA or with no treatment as basal and incubated for 10 mins at 37°C. After incubation, the red blood cells were lysed for 15 mins at room temperature while protected from light. Then, the cells were washed twice and centrifuged at 1400 RPM for 3 mins. Finally, cells were resuspended with 1 mL of PB buffer and were examined on a Beckman flow cytometer (CytoFLEX LX). 50,000 events were acquired for each sample. Human monocyte population was identified by forward and side scatter and the expression of CD14.

**Mouse study -** APP/PS1 transgenic mouse is widely used as an animal model of AD. These mice start to accumulate Aβ in brain from 4 months; however, cognitive impairment only becomes evident from 10 months, and the lifespan is between 25–27 months. To better resemble the human AD, we used 22–24 months old female AD mice for this study. All animals underwent surgery to implant the mini-osmotic pump (ALZET, model 1004, 100μL reservoir volume, four weeks duration) plus ALZET Brain Infusion Kit 3. GA (20 mg/mL) (n = 9) or the control (isotonic saline containing 4% mannitol; n = 7) were loaded into minipump (100 μL each). Animals were anaesthetised with isoflurane inhalation and implanted with the mini-osmotic pump in the subcutaneous space in the back, penetrating 2.5 mm below the skull surface, which is appropriate for targeting the lateral ventricles in an adult mouse. The whole procedure followed the instruction as described previously (13). The reagents were expected to be released slowly within four weeks.

Mice underwent behavioural testing in the open field, elevated plus maze, Y maze, rotarod and social interaction over two consecutive weeks beginning at the 22th day after treatment. In the second week of behavioural testing includes rotarod and social interaction, three mice dropped off successively due to natural death or humane endpoint. Behavioural testing was conducted by an experimenter blinded to group assignment. Behaviour was recorded by an overhead camera, and behavioural metrices were objectively quantified using EthoVision tracking software (Noldus, Leesburg, VA, USA). To assess locomotion and anxiety-like behaviour, mice were tested in an open-field as previously described (14–16). Briefly, the mouse was placed in the center of the open-field and allowed to freely explore the arena for 5 minutes. The total distance moved, number of entries into the inner area of the maze, and time spent in the inner area of the maze were measured. Elevated plus maze (EPM) was used to evaluate anxiety-like behaviour, based on the tendency of rodents to avoid open spaces. During a 10 min period, mice were permitted free exploration of the apparatus, which consists of 2 open arms and 2 enclosed arms (San Diego Instruments, San Diego, USA). Distance moved and time spent in the open arms, as a percentage score, calculating by the time spent in the open arm/[time in open arm + time in closed arm], were examined. Spatial cognition was assessed in the Y maze as previously described. The Y-shaped apparatus consists of three enclosed arms of equal dimensions (San Diego Instruments, San Diego, USA), each with a different visual cue at the distal end. First, a 15-min habituation trial was conducted, in which the mouse was able to freely explore two arms while the third arm was blocked from access. After a 2-h interval, the third arm was unblocked, and a 5-min test trial was conducted, in which the mouse was able to freely explore all three arms. The number of entries into the novel and familiar arms and total distance travelled were determined. The three-chamber paradigm is a test to evaluate same-sex social affiliation and social recognition in mice. The task was performed as described previously (16). The apparatus has a central chamber and two outer chambers. Same-sex, age-matched, naive stimulus mice were restricted to rectangular metal cages fitted at one end of the outer chambers, such that experimental mice could only approach and initiate a social investigation from one side. Testing consisted of three consecutive 10-min stages: (1) habituation in the chamber, containing two empty cages; (2) a choice between an empty cage and a cage containing a stimulus mouse; and (3) a choice between a second ‘novel’ stimulus mouse and the first, now ‘familiar’ mouse. Stages 2 and 3 are measures of the subject’s

preference for sociability and social recognition/social memory, respectively. Stimulus mice and their relative positioning (left versus right chambers) were randomised between subjects. Data were expressed as time spent in each of the outer chambers as a percentage of total time. The rotarod was used to assess motor function as previously described (15). The apparatus consisted of a rotating barrel divided by walls into four equal lanes (Harvard Apparatus, Holliston, TX, USA). Three trials were performed each day for two consecutive days (day 1 = training, day 2 = testing). For each trial, the mouse was placed on the rotating barrel, the speed was accelerated from 0.0027 to 0.27 g (4 to 40 RPM) at a rate of 0.00017 g/8 s, and the duration of time on the rotarod that the mouse was able achieve was recorded (maximum time of 5 minutes).

Following the completion of these behavioural tests, mice were euthanized, and the brain were collected for LTP measurement, immunohistochemical tests and Aβ quantification.

# Histology and Immunohistochemistry

Mouse brains (GA, n = 4 and Controls, n = 4) were perfusion fixed with 4% paraformaldehyde and then placed in 10% neutral buffered formalin prior to standard histological processing for paraffin embedding and sectioning (5 µm). A survey section was deparaffinised and stained with haematoxylin and eosin.

Sections for Aβ (Dako MO872–clone 6F/3D) and microglia (Abcam ab178846) immunohistochemistry (IHC) were deparaffinised, rehydrated, and endogenous peroxidase blocked with 5% aqueous hydrogen peroxide (5 min). The sections for Aβ IHC were treated with 98–100% formic acid (Scharlau AC10852500) for 5 min, rinsed in water, and immersed in Tris buffer (0.5M pH 7.6) before a 1/100 dilution of MO872 was applied for 60 mins at room temperature. Sections for microglial IHC didn't require antigen retrieval and the primary antibody was diluted 1 in 2000 in Tris and applied for 60 mins.

Positive labeling was detected with a peroxidase labeled streptavidin/biotin system (Dako K0675) with a diaminobenzidine chromogen. Sections were counterstained with Harris's haematoxylin, dehydrated and coverslipped. Low and high magnification images were obtained with a Leica ICC50 HD camera on a Leica DM 750 binocular microscope. We then analyzed Aβ IHC with whole mount view (4X) by dissecting the brain section into hippocampal area (Suppl. Figure 3a) and cortical area (Suppl. Figure 3c). Aβ plaque structures were isolated and analyzed in Suppl. Figure 3b and d by method described elsewhere (17). We also analyzed microglial IHC sections (20X) based on method described previously (18). For Aβ IHC, the sections of two samples were not ideal in presentation of the hippocampal areas because of the positioning angle, and they were excluded from the quantitative analysis.

# ELISA Aβ quantification

The Aβ levels were determined using the sandwich ELISA described previously (19). The assay was conducted in 384 well, high-binding polystyrene plate (Greiner). The plate was precoated with 25 µL of 10 µg/ml W0-2 monoclonal antibody (epitope Aβ 5–8) in 50 mM sodium carbonate, pH 9.6, at 4°C overnight. After washing with PBST (PBS containing 0.05% Tween), the plate was blocked with 0.5% (w/v) casein in PBS buffer, pH 7.4, to minimize nonspecific binding, and washed with PBS before addition

of samples (in triplicate) and 1E8-biotin (epitope 17–22, final concentration 0.3 ng/ml) and incubated overnight at 4°C. The plate was washed with PBST and europium-labelled streptavidin (final concentration 1 nM) added for 1 hr at room temperature. After a final wash, the plate was developed with a commercial enhancement solution, and read using the Wallac Victor2 1420 Multilabel Plate Reader (PerkinElmer, Melbourne, Australia) with excitation at 340nm and emission at 613nm. The values obtained from the triplicated wells were used to calculate the Aβ concentration (expressed as ng/ml) based on the standard curve generated on each plate.

**Rabbit study -** Healthy female New Zealand White rabbits (2.7–4.6 kg) aged 12–15 weeks (n = 7) were purchased from a commercial rabbit breeding facility. Rabbits were randomized for various experimental purposes. They were housed in pairs or separately in a room kept at 21$^{o}$C with a 12h light dark cycle. Rabbits were placed in a polycarbonate box and received local anaesthetic applied on ears subcutaneously (50/50 mix of 1% lignocaine + 1% ropivacaine with 30-gauge needle). YG beads (1.5 mL) was injected intravenously via marginal ear vein at a rate of 1.0 mL/ minute. After 5 min, GA at a dose of 2 mL/kg or PBS with 4% mannitol was injected into the marginal ear vein at a rate of 1 mL/ minute. Sample blood (200 µL) was collected from central ear artery of the other ear 5 min before bead injection as the baseline, followed by multiple collections at 5, 10, 15, 20, 30, 60 and 120 min after administration of GA or PBS. Blood samples were incubated with 4 mL of BD lysing solution for 15 min on ice, followed by washing with PBS and incubation with Alexa 647 conjugated anti rabbit CD14 mAb for 15 min. Cells were washed in PBS and the samples were analyzed by a BD FACSCalibur flow cytometry in gated $CD14^{+}$ monocyte and $CD14^{-}$ neutrophil population.

**Sheep study -** In order to further verify the drug safety and obtain pharmacokinetic data, three adult sheep were selected for introductory experiments (36.5, 35.8 and 48.6 kg respectively). Ventricular cannulation (Intra-cerebroventricular surgery, ICV) was performed on sheep according to previously described methods (20). To test for GA drug safety, on the first day after the ICV operation, we injected 1 mL of carrier solution (4% mannitol in artificial cerebrospinal fluid, sterilized and filtered) from the ICV catheter at a rate of 0.5 mL/min (same rate for all the following injections). Cerebrospinal fluid (0.5 mL), blood (5 mL), and urine (5 mL) samples were collected to establish a baseline. GA was then injected once a week for 8 weeks at a dose of 10 mg in 0.5 mL. Heartbeat and breathing, anal temperature, forage consumption, drinking, defecation and urination were recorded daily.

To study the pharmacokinetics of GA, Alexa488 and Alexa647 conjugated GA was prepared using the conjugation kit (Thermo Fisher Scientific Australia) according to the manufacture's instruction, the concentration was determined by Direct Detect (Merck), and the standard concentration curves were established with fluorescence spectrophotometry. Alexa488 or Alexa647 conjugated GA (10 mg) was injected via ICV. Cerebrospinal fluid (0.5 mL each time) was collected through intraventricular catheters, blood samples (5 mL each time) was collected through an external jugular vein cannulation, urine samples (5mL each time) was also collected, before GA injection and 0.5, 1, 2, 4, 8, 24, 48 and 72 hours after injection. The fluorescence intensity in each sample was measured and calculated with the standard curves.

# Data analysis and statistics

Flow cytometry results were analyzed using FlowJo™ v10.8 Software (BD Life Sciences). Data analyzes and plotting were done using GraphPad Prism for Windows (Version 9.0, San Diego, California USA) or IBM SPSS Statistics for Windows (Version 28.0, Armonk, NY: IBM Corp.). For LTP assay, as there was no difference of basal fEPSPs between different treatment groups, a One-Way ANOVA was employed in comparison of LTP among different groups and the level of statistical significance was set up at $p < 0.05$. Two-way multivariate analyzes of variance (ANOVAs) were performed for social interaction and rotarod, with independent variables of treatment and chamber side (for social interaction) or treatment and day/training (for rotarod), and a (repeated) dependent variable of time, as appropriate. Triplicate values for each animal (for rotarod) were averaged before analyzing the data. Multiple comparisons were performed by Bonferroni-Šídák test and are annotated graphically where significant.

# Results

**GA promotes innate phagocytosis** in vitro **and** in vivo

Previously we have shown that GA enhances innate phagocytosis by peripheral monocytes *in vitro* (8). In this study, we confirmed this finding by using YG beads instead of YO beads (Fig. 1a), and by using mouse monocytes instead of human ones (Fig. 1b). To test its effect *in vivo*, rabbits were injected intravenously with 1.5 mL YG beads followed by injection of 2 mL/kg GA or 4% mannitol as control. Following the injection of GA, a temporary enhanced phagocytic activity in $CD14^+$ monocytes was found in a time-dependent manner, with 30 minutes being the peak (Fig. 1c-d). In contrast, $CD14^-$ neutrophils also phagocytosed small amount of YG beads; however, no significant difference was found between the GA and the control groups (Fig. 1e-f). This is consistent with *in vitro* findings that GA did not alter phagocytosis by neutrophils. As neutrophils are major regulatory cells in the adaptive immune system due to their high expression of Fc receptors, e.g. CD16, CD32 and CD64., our finding indicates that the phagocytosis-promoting effect of GA may have a major effect in the innate immune system only.

# GA promotes Aβ absorption to monocytes

The mechanism of cerebral Aβ clearance by microglia/monocytes, which potentially involves endocytosis, phagocytosis and autophagy, is still unclear. Recognition of Aβ or Aβ/ApoE complex by monocytes is the first step. We therefore studied the effect of GA on Aβ adhesion to leukocyte surface. Whole blood (n = 6) was incubated with synthetic Aβ in the presence and absence of GA. Monocytes showed high Aβ adhesion, which was enhanced marginally in the presence of GA compared to Aβ alone (Aβ + GA *vs.* Aβ, Fig. 1g, Tukey HSD test, adjusted P = 0.06), while lymphocytes and neutrophils only showed slight Aβ adhesion which was not affect by GA. Monocytes were then stratified into three subsets based on CD14 and CD16 expression. Results showed that intermediate monocytes ($CD14^+CD16^+$) are a dominant subset for Aβ adhesion, followed by the $CD14^{dim}CD16^+$ non-classic monocytes, while classic monocytes ($CD14^+CD16^-$) only showed similarly low levels of Aβ adhesion as lymphocytes and neutrophils (Fig. 1h). In the presence of GA, intermediate monocytes showed a significant increase of Aβ

adhesion when compared with Aβ alone (Aβ + GA vs. Aβ, Fig. 1h, Tukey HSD test, adjusted P = 0.03). For non-classic monocytes, the effect of GA was not statistically significant, and for classic monocytes, no effect was observed (Fig. 1h).

# GA binds Aβ with a high affinity

In order to determine whether there is an interaction between GA and Aβ, we employed circular dichroism (CD), which can determine whether there are changes in the conformation of peptides when they interact (21). CD spectra were acquired for individual Aβ monomer and GA, as well as the complex of two (Fig. 2a-c). The results showed a β-sheet preferred structure of Aβ but was less obvious for GA. The complex presented a clearly different structure, indicating an interaction between GA and Aβ (Fig. 2d).

Microscale thermophoresis (MST) was then used to determine binding affinity between GA and Aβ peptides. The thermophoresis signal was plotted against the GA concentration to obtain a dose-response curve, from which the binding affinity was deducted (Fig. 2e). Freshly dissolved $A\beta_{1-42}$ peptides (mostly in monomer form) showed an extremely low dissociation constant of $K_d = 6.6 \times 10^{-9}$ M with GA, while for aged Aβ (dissolved and left at 4°C for 7 days) the value was $2.54 \times 10^{-8}$ M, indicating a high affinity between GA and Aβ as compared with the reported affinity of aducanumab to Aβ monomer ($10^{-6}$ M) (22).

We further studied the high affinity between GA and Aβ using Western blotting. Synthetic $A\beta_{1-42}$ was mixed with an escalating amount of GA by molar ratios 1:0–7, and the mixtures were then subjected to SDS-PAGE in a reduced condition. GA significantly retarded Aβ in electrophoresis in a dose-dependent manner, even under reduced and heated conditions (Fig. 2f-g), suggesting a tight and irreversible binding between GA and Aβ.

# GA antagonizes cytotoxicity of Aβ

We then examined whether GA was able to inhibit Aβ toxicity on neuronal cells. SH-SY5Y cell viability assay using MTT system was performed. MTT is reduced to pigmented formazan by live cells and therefore the absorbance of formazan is proportional to the number of living cells. It was found that addition of 10 μM $A\beta_{1-42}$ reduced 45.0 ± 0.1% cell viability in comparison to the control. GA neutralized this neurotoxic effect of Aβ in a dose-dependent manner (ANOVA P < 0.0001) with 70 μM being the highest (unpaired T test, P = 0.019) (Fig. 3a).

Long-term potentiation (LTP) represents the long-lasting increase in signal transmission between neurons within a distance. LTP recording is a widely recognized cellular model for the study of learning and memory. In a freshly prepared acute brain slice from naïve C57/BL6 mice, $A\beta_{1-42}$ (1 μM) was found to reduce LTP in comparison to artificial CSF (aCSF) control (Fig. 3c Aβ:120 ± 5% *vs* aCSF:138 ± 4%, P = 0.0003). GA (50 or 100 μg/mL) alone did not affect LTP, however, when Aβ was co-perfused with GA, GA completely blocked Aβ-induced LTP suppression in a dose-dependent manner, even elevating LTP over the level of the control (aCSF) (Fig. 3c GA 50 + Aβ: 143 ± 7% (P < 0.01) and GA 100 + Aβ: 168 ± 7%, P < 0.001).

The results of cell viability and LTP recording suggest Aβ could disturb cell membrane. We then further investigated the effect of Aβ on membrane disruption of human monocytes by using a fluorescent lipophilic probe, TMA-DPH (Fig. 3d-e). In about 1/4 of our tested subjects, the membrane fluidity of $CD14^+$ monocytes were elevated in the presence of 5 μM Aβ monomer (Paired T test, P = 0.03), and GA at a concentration of 100 μg/mL neutralized this effect (Paired T test, P = 0.04).

# Intracerebroventricular delivery of GA ameliorates anxiety-like behaviour and improves cognitive function of AD mice

We examined the effect of GA in aged APP/PS1 mice (average 23 months old) using direct brain infusion via implantation of mini-osmotic pumps (Suppl. Figure 1). GA (100 μL of 20 mg/mL) was loaded into the pump and released slowly over the next 28 days, averaging 71 μg/day. Mice (GA: n = 9 and Control: n = 7) underwent behavioural testing, including the open field, elevated plus maze (EPM), Y maze, social interaction and rotarod, over two consecutive weeks beginning 22 days after implantation of minipumps with GA or vehicle. Within an anxiety-like behaviour test like open field or EPM, a normal mouse avoids an open area. We found that both GA and control animals showed normal preference to the sheltered areas. Comparably, GA mice stayed significantly longer time in the open areas, presenting as % time in the center (for open field) or % time in the open arms (for EPM), when compared with controls (Fig. 4a and b, Unpaired T test, P = 0.04 and P = 0.02, correspondingly), suggesting that GA treated mice had less stress and more interest in novel environment exploration. These findings were not confounded by hyper- or hypo-activity (Suppl. Figure 2a). Spatial cognition was assessed in the Y maze and the GA mice spent significantly longer time in the novel arm when compared with controls (Fig. 4c, Unpaired T test, $P < 0.05$), indicating that the GA treated mice have improved pattern recognition and working memory. Social affiliation and social recognition were evaluated in a classic three-chamber paradigm. No preference was found between left and right chambers (Suppl. Figure 2b, two-way ANOVA, $F_{1,9} = 0.01$, P = 0.94) in Stage 1. Both GA mice and controls showed preference to the stimulus chamber over the empty chamber in Stage 2 (Fig. 4d, two-way ANOVA, $F_{1,9} = 10.1$, P = 0.01). No group difference was found (two-way ANOVA, $F_{1,9} = 2.2$, P = 0.17); Whereas a *post-hoc* multiple comparison test showed that GA mice were tending towards stimulus chamber which reached significance (Bonferroni-Šídák test, adjusted P = 0.03); while controls did not (Bonferroni-Šídák test, adjusted P = 0.22). Similarly, both groups showed preference to the new stimulus chamber over the old stimulus chamber in Stage 3 (Fig. 4e, two-way ANOVA, $F_{1,9} = 15.80$, P = 0.003). No group difference was found (two-way ANOVA, $F_{1,9} = 0.18$, P = 0.68). Multiple comparison test showed that two groups had similar preference towards new stimulus chamber (Bonferroni-Šídák test, controls adjusted P = 0.04 and GA adjusted P = 0.04). Further, the lack of group difference in the rotarod (Fig. 4f, two-way ANOVA, $F_{1,26} = 0.00$, P = 0.99) demonstrates that the observed differences between GA and control animals in other tasks were unlikely to be influenced by potential differences in sensorimotor function.

At the completion of the behavioural studies, mice were euthanised. Fresh brain slices were prepared for *ex vivo* LTP assay. The control mice showed typical LTP suppression by brain Aβ; whilst GA treated mice

showed restored LTP function (Fig. 5a, unpaired T test, $P < 0.0001$), implicating a recovery in the memory and learning capacity in these aged AD mice. This is consistent with the Y maze test results described above. Moreover, the concentration of brain soluble Aβ decreased from 39 ± 25 pg/mg protein in the GA mice to 26 ± 13 pg/mg protein in the control mice (Fig. 5c, unpaired T test, $P = 0.20$). Although the difference was not statistically significant, the ratio between soluble Aβ and insoluble Aβ decreased from 0.40% in the GA group to 0.29% in the control group (Fig. 5d, Unpaired T test, $P = 0.02$), as did the percentage of soluble Aβ in total Aβ (Fig. 5e, unpaired T test, $P = 0.02$).

We further examined mouse brain sagittal sections by immunohistochemical staining for Aβ plaques and microglial cells. Aβ staining showed reduced number of plaques in the hippocampal area (Fig. 5f) and reduced average size of plaques in the cortical area (Fig. 5h) in the GA group compared with the control. Interestingly, etching ring shape plaques (suppl. Fig. S4) were found in all GA treated mice, mostly in the cortex regions. In contrast, the control mice brain slices show large and diffused plaques (suppl. Fig. S4). This unique shape of plaques may represent Aβ plaque dissolving by phagocytosis in the GA-treated mice.

The immunostaining results of IBA-1 showed that compared with the controls, GA treated mice had increased number of microglia in cortex and hippocampus regions (unpaired T test, $P = 0.02$ and $P < 0.01$, respectively), which had longer branch length ($P < 0.0001$ and $P = 0.02$, respectively) and more endpoints/branches ($P < 0.0001$ and $P = 0.02$, respectively) (Fig. 5i-k). These results imply that these microglia in GA treated mice are more like in a non-inflammatory ramification state.

# Intracerebroventricular delivery of GA greatly promotes energy metabolism

Further examination of the biological effect and safety of GA was carried out on Australian adult sheep. Intracerebroventricular cannulas were implanted in the sheep head as previously described (20). One week later, GA (0.5 mL of 20 mg/mL) was administered via cannula once per week for eight weeks. We found that within 24 hours after each GA injection, the body temperature generally increased by 0.5$^{o}$C; however, the average body temperature was maintained between 37.8-39.5$^{o}$C throughout the experiment (Fig. 6). Soon after GA injection, the most obvious change was that the animal's food intake had increased greatly. Forage consumption increased from 400–800 grams to 800-2,400 grams, and sometimes even more than 3000 grams per day. Water consumption increased from the initial volume of less than 4 litres to 8–16 litres per day. At the same time, excretion also increased greatly: faecal excretion increased by an average of 1–2 times, while urination increased from 2–3 litres per day to a full bucket of 12 litres (Fig. 6). This phenomenon was observed in all three animals and continued till 2–3 weeks after the last injection, showing that intracerebroventricular injection of GA greatly stimulated the animals' metabolism. It is worth noting that we checked the blood routine (FBC, CRP, blood biochemistry, preserved glucose (FLOX), glycated haemoglobin (HbA1c)), thyroid studies (total T4 and TSH)), urine routine, liver function, kidney function of the animals, and there were no abnormalities or significant changes (data not shown). The animals' weights did not increase. Meanwhile, pharmacokinetic tests with

fluorophore labelled GA (Suppl. Fig. S5) showed that GA concentration in the CSF dropped rapidly after 24 hours and almost completely disappeared at 48 hours; while the GA concentration in the blood increased after 24 hours and lasted at least 72 hours. However, no reliable results were obtained in the urine due to its strong fluorescent background.

# Discussion

In the current study, we have demonstrated that GA can form a complex with Aβ peptides. This complex abolishes neurotoxicity of Aβ and restores LTP of hippocampus from wild type mice. In contrast, GA alone does not affect LTP levels. Similarly, accompanied with improved cognitive behavioural tests by chronic treatment of GA, hippocampal LTP in aged APP/PS1 mice was also significantly elevated. The mechanism underneath the elevated LTP by GA is not clear but a reduction of brain Aβ burden by GA could not be excluded.

In most cases of sporadic AD, Aβ accumulation is associated with deficiencies in clearance (23, 24). It is estimated that up to 60% of brain Aβ is removed to peripheral blood and lymphatic systems while the rest is degraded inside the brain (25, 26). In the parenchyma, professional phagocytes such as microglia, together with astrocytes and neurons, are responsible for the catabolism of Aβ (27). Myelomonocytic cells, including resident microglia and infiltrating monocytes, have been shown to phagocytose fibrillar Aβ and perhaps soluble oligomers as well. Mounting evidence from genetic associations, with hits such as *ABCA7*, *CD33*, *CLU*, *CR1*, *MS4A* and *TREM2* (28–32), have implicated innate phagocytosis pathways in sporadic AD. Variants of these genes, especially CD33 and TREM2, are associated with a compromised phagocytic function of microglia/monocytes and altered Aβ accumulation in AD brains (33, 34). In the CNS, innate phagocytosis mediated by microglia is responsible for recognition and engulfment of cell debris, protein aggregates and invading bacteria (8, 35). Unlike the adaptive immune response, innate phagocytosis does not rely on antibody or complement system, but is inhibited by as little as 1% serum, an effect which is mediated by copper-containing glycoproteins (36). Thus, innate phagocytosis has maximal activity in the brain where cerebrospinal fluid (CSF) is free of plasma proteins. Moreover, as innate phagocytic function is reduced with aging (35, 37), it should be considered as one of the most likely pathogenic mechanisms underlying age-related neurodegenerative disorders, such as AD (8) and age-related macular degeneration (AMD) (9). Promoting innate phagocytosis could therefore be an effective strategy for age-related neurodegeneration.

AD patients may experience behavioural and personality changes such as: irritability, anxiety and depression. Other symptoms may occur including agitation, emotional distress, hallucinations, sleep issues and sundowning (38). With both of open field and EPM measuring of anxiety-like behaviour, GA significantly increased the time spent in the open areas as compared to controls. GA significantly increased the time spent in the novel arm in the Y maze as compared to controls, suggesting even cognitive decline may be partially reversible if removing abnormally accumulated Aβ. Furthermore, GA did not alter the fall down latency in the rotarod. Our findings indicated that GA exerts both anxiolytic and cognition-protecting without altering the motor coordination.

Compared with matched controls from the general population, the weight and body mass index of AD patients decreased significantly (39). It has been reported that high levels of Aβ may damage hypothalamic arcuate neuropeptide Y neurons and down-regulate leptin status in the early stages of the disease, which may lead to weight loss (40, 41). People with advanced AD may lose the feeling of hunger and thirst, and orexigenic peptides such as neuropeptide Y have been proposed to treat AD by stimulating appetite (42, 43). The results from our sheep study indicated that GA may well be one of the orexigenic peptides as well, and be able to greatly promote brain energy metabolism, which is needed for our brain to fight against cognitive decline (44). It is intriguing that NPY that increases hunger can also promote the phagocytic function of mouse macrophages *in vitro*, while another neuropeptide that increases satiety, cholecystokinin octapeptide (CCK-8), can inhibit the phagocytic function (45, 46).

The activity of the brain consumes 25% of the body's glucose and 20% of the oxygen, although the brain only accounts for 2% of the total body weight (47, 48). Some small changes in brain energy metabolism may disrupt brain function and cause neurodegenerative diseases, such as AD (49–51). As a unique phagocyte in the brain, microglia constantly move their processes, patrol the brain, and make dynamic contact with neuronal somata and synapses (52). The functions performed require high energy consumption (53). Microglia dysfunction, especially neuroinflammation, is an important participant in degenerative neurological diseases. These diseases are accompanied by changes in brain energy metabolism and continuous inflammation, and energy metabolism has a strong influence on the inflammatory response of microglia. In our mouse experiments, GA treatment assisted microglia to clear amyloid plaques in the brain. More microglia may be derived from the proliferation of cells. These cells are obviously at “resting” mode and have more cell protrusions. Compared with the cells in the control group, there is no obvious inflammatory response, indicating that GA can promote the phagocytic function of microglia, inhibit inflammation, and protect the function of neuronal cells. In the sheep experiment, we found that GA injection can increase the appetite of the sheep and increase the food/water intake. This mechanism may just meet the needs of brain repair and the functional activity of microglia, therefore we did not see weight gain in these sheep.

GA is an FDA-approved drug used to treat relapsing forms of multiple sclerosis. It has proven biosafety when administered subcutaneously. Our mouse, rabbit and sheep studies also demonstrated the safety of GA when administered intravenously or intracerebroventricularly. The *in vivo* dose we used was much higher than the *in vitro* effective dose (100 μg/mL). For example, an aged APP/PS1 mouse weighing 35–40 g has about 35 μL CSF, the concentration of GA was therefore ~ 2 mg/mL; for adult rabbit weighing around 3.5 Kg, blood volume is about 60 mL, GA concentration would be ~ 0.6 mg/mL; for sheep weighing around 40 Kg, the CSF volume is around 14 mL, so it would be ~ 0.7 mg/mL. With these high doses, we did not observe any abnormality except temporary weight loss (< 20%) in mice shortly after surgery. GA also has limited capacity to pass through the BBB from the CNS to periphery, as shown by our pharmacokinetic study; however, whether it can infiltrate from periphery to CNS requires further investigation. Theoretically, although GA can be delivered to the human brain (e.g., through lumbar puncture, nasal spray, or implantation of devices such as Ommaya shunt, which is a broadly used intraventricular catheter system implanted under the scalp for delivery of drug into the cerebrospinal

fluid), a smaller molecule which promotes phagocytosis and binds to Aβ would be more suitable for clinical practice.

# Conclusion

In this study, we have shown that GA promotes innate phagocytosis and tightly binds Aβ, which facilities the clearance of Aβ in the brain and improves cognition and metabolism. Our proof-of-concept study inspires a new treatment strategy for early and advanced AD.

# Abbreviations

aCSF
Artificial CSF
AD
Alzheimer's disease
AMD
Age related macular degeneration
ARIA
Amyloid-related imaging abnormalities
Aβ
Amyloid β peptide
BBB
Blood-brain barrier
CD
Circular dichroism
CNS
Central nervous system
CRP
C-reactive protein
CSF
Cerebrospinal fluid
DMSO
Dimethyl sulfoxide
ELISA
Enzyme-linked immunosorbent assay
EPM
Elevated plus maze
FBC
Full blood count
FDA

U.S. Food and Drug Administration
fEPSPs
Field excitatory postsynaptic potentials
FLOX
Sodium fluoride/potassium oxalate blood collection tube
GA
Glatiramer acetate
HFS
High frequency stimulus
ICV
Intracerebroventricular drug delivery
LTP
Long-term potentiation in the hippocampus
MEA
Multi-electrode array electrophysiology
MST
Microscale thermophoresis
MTT
(3-(4,5-dimethylthiazol-2-yl)-2,5-diphenyltetrazolium bromide
SDS-PAGE
Sodium dodecyl sulphate–polyacrylamide gel electrophoresis
T4
Thyroxine
TMA-DPH
Trimethylammonium-diphenylhexatriene
YG beads
Yellow green carboxylate microspheres
YO beads
Yellow orange carboxylate microspheres

# Declarations

**Ethics approval and consent to participate:** The mouse study was approved by the Florey Institute Animal Ethics Committee (16-076 and 17-032). The sheep study was approved by the Flory Institute Animal Ethics Committee (18-010). The rabbit experiment received approval from the Florey Institute Animal Ethics Committee (13-054, 14-011 and 15-037). Human blood samples were collected in clinic which meets the appropriate ethical standards of the Human Research Ethics Committee, St Vincent's Hospital, Melbourne (Ref: HREC-A 028/06) and the Eastern Health Research and Ethics Committee (Ref: E05/1011). All participants and patient caregivers completed written informed consent before participation.

**Consent for publication:** We, the undersigned, give our consent for the publication of identifiable details, which can include photograph(s) and/or details within the text (“Manuscript”) to be published in the above Journal.

**Availability of data and materials:** All data generated or analysed during this study are included in this published article and its supplementary information files.

**Competing interests:** The authors declare that the research was conducted in the absence of any commercial or financial relationships that could be construed as a potential conflict of interest.

**Funding:** This work was supported by ARC Future Fellowship (BG, FT120100581) and NHMRC Project Grant (1048082, 1061419, 1120095, and 110178 to BG), Macular Disease Foundation (2014-2016 and 2017-2018 to BG), BrightFocus Foundation (M2016061 to BG) and the Victorian Government's Operational Infrastructure Support Grant to the Florey Institute and St. Vincent’s Institute. MWP is an NHMRC Leadership Fellow (1194263). Qiankang Life Science Melbourne R&D Centre sponsored the sheep study. None of the funding sources was involved in this study.

**Authors’ Contributions:** XH, mouse and sheep surgery, in vitro cell biological assays, behaviour tests, writing; FC&PA, LTP; LD&MWP, affinity assays; QL, Aβ quantitation; IB, immunohistochemical staining; CD&AA: membrane fluidity; MJ, BD, SS, behaviour tests; WO, rabbit experiments; YL, JW, KP & ML: sheep experiments; MM, sheep surgery; CLM&JSW, writing and results interpreting; BJG, design, animal experiments, affinity assays, writing.

**Acknowledgement:** MST was accessed through the Bio21 Melbourne Protein Characterisation platform. We thank A/Prof. Christine E. Wright and Ms. Linda Cornthwaite-Duncan for their great help in the rabbit study; We thank Mr. Alan McDonald, Mr. Tom Vale, Dr. Ameen Farsakh and Mr. Pavan Avula for assistance in animal surgery and monitoring, and Dr. Shijie Liu and Dr. Kyria Webster for assistance with mouse surgery and behavioural testing.

# References

1. Doody RS, Thomas RG, Farlow M, Iwatsubo T, Vellas B, Joffe S, et al. Phase 3 trials of solanezumab for mild-to-moderate Alzheimer's disease. N Engl J Med. 2014;370(4):311–21.
2. Salloway S, Sperling R, Fox NC, Blennow K, Klunk W, Raskind M, et al. Two phase 3 trials of bapineuzumab in mild-to-moderate Alzheimer's disease. N Engl J Med. 2014;370(4):322–33.
3. Sevigny J, Chiao P, Bussiere T, Weinreb PH, Williams L, Maier M, et al. The antibody aducanumab reduces Abeta plaques in Alzheimer's disease. Nature. 2016;537(7618):50–6.
4. Frenkel D, Maron R, Burt DS, Weiner HL. Nasal vaccination with a proteosome-based adjuvant and glatiramer acetate clears beta-amyloid in a mouse model of Alzheimer disease. J Clin Invest. 2005;115(9):2423–33.

5. Butovsky O, Koronyo-Hamaoui M, Kunis G, Ophir E, Landa G, Cohen H, et al. Glatiramer acetate fights against Alzheimer's disease by inducing dendritic-like microglia expressing insulin-like growth factor 1. Proc Natl Acad Sci U S A. 2006;103(31):11784–9.
6. Koronyo Y, Salumbides BC, Sheyn J, Pelissier L, Li S, Ljubimov V, et al. Therapeutic effects of glatiramer acetate and grafted CD115(+) monocytes in a mouse model of Alzheimer's disease. Brain. 2015;138(Pt 8):2399–422.
7. Dionisio-Santos DA, Karaahmet B, Belcher EK, Owlett LD, Trojanczyk LA, Olschowka JA, et al. Evaluating Effects of Glatiramer Acetate Treatment on Amyloid Deposition and Tau Phosphorylation in the 3xTg Mouse Model of Alzheimer's Disease. Front Neurosci. 2021;15:758677.
8. Gu BJ, Huang X, Ou A, Rembach A, Fowler C, Avula PK, et al. Innate phagocytosis by peripheral blood monocytes is altered in Alzheimer's disease. Acta Neuropathol. 2016;132(3):377–89.
9. Gu BJ, Huang X, Avula PK, Caruso E, Drysdale C, Vessey KA, et al. Deficits in Monocyte Function in Age Related Macular Degeneration: A Novel Systemic Change Associated With the Disease. Front Med (Lausanne). 2021;8:634177.
10. Ida N, Hartmann T, Pantel J, Schroder J, Zerfass R, Forstl H, et al. Analysis of heterogeneous A4 peptides in human cerebrospinal fluid and blood by a newly developed sensitive Western blot assay. J Biol Chem. 1996;271(37):22908–14.
11. Rogers J, Chen F, Stanic D, Farzana F, Li S, Zeleznikow-Johnston AM, et al. Paradoxical effects of exercise on hippocampal plasticity and cognition in mice with a heterozygous null mutation in the serotonin transporter gene. Br J Pharmacol. 2019;176(17):3279–96.
12. Malakooti N, Pritchard MA, Chen F, Yu Y, Sgambelloni C, Adlard PA, et al. The Long Isoform of Intersectin-1 Has a Role in Learning and Memory. Front Behav Neurosci. 2020;14:24.
13. Claflin KE, Sandgren JA, Lambertz AM, Weidemann BJ, Littlejohn NK, Burnett CM, et al. Angiotensin AT1A receptors on leptin receptor-expressing cells control resting metabolism. J Clin Invest. 2017;127(4):1414–24.
14. Bao F, Shultz SR, Hepburn JD, Omana V, Weaver LC, Cain DP, et al. A CD11d monoclonal antibody treatment reduces tissue injury and improves neurological outcome after fluid percussion brain injury in rats. J Neurotrauma. 2012;29(14):2375–92.
15. Shultz SR, Sun M, Wright DK, Brady RD, Liu S, Beynon S, et al. Tibial fracture exacerbates traumatic brain injury outcomes and neuroinflammation in a novel mouse model of multitrauma. J Cereb Blood Flow Metab. 2015;35(8):1339–47.
16. Semple BD, Dixit S, Shultz SR, Boon WC, O'Brien TJ. Sex-dependent changes in neuronal morphology and psychosocial behaviors after pediatric brain injury. Behav Brain Res. 2017;319:48–62.
17. Crowe AR, Yue W. Semi-quantitative Determination of Protein Expression using Immunohistochemistry Staining and Analysis: An Integrated Protocol. Bio Protoc. 2019;9(24).
18. Young K, Morrison H. Quantifying Microglia Morphology from Photomicrographs of Immunohistochemistry Prepared Tissue Using ImageJ. J Vis Exp. 2018(136).

19. Ryan TM, Roberts BR, McColl G, Hare DJ, Doble PA, Li QX, et al. Stabilization of nontoxic Abeta-oligomers: insights into the mechanism of action of hydroxyquinolines in Alzheimer's disease. J Neurosci. 2015;35(7):2871–84.
20. McKinley MJ, Denton DA, Park RG, Weisinger RS. Ablation of subfornical organ does not prevent angiotensin-induced water drinking in sheep. Am J Physiol. 1986;250(6 Pt 2):R1052-9.
21. Sreerama N, Woody RW. Estimation of protein secondary structure from circular dichroism spectra: comparison of CONTIN, SELCON, and CDSSTR methods with an expanded reference set. Anal Biochem. 2000;287(2):252–60.
22. Arndt JW, Qian F, Smith BA, Quan C, Kilambi KP, Bush MW, et al. Structural and kinetic basis for the selectivity of aducanumab for aggregated forms of amyloid-beta. Sci Rep. 2018;8(1):6412.
23. Mawuenyega KG, Sigurdson W, Ovod V, Munsell L, Kasten T, Morris JC, et al. Decreased clearance of CNS beta-amyloid in Alzheimer's disease. Science. 2010;330(6012):1774.
24. Wang J, Gu BJ, Masters CL, Wang YJ. A systemic view of Alzheimer disease - insights from amyloid-beta metabolism beyond the brain. Nat Rev Neurol. 2017;13(10):612–23.
25. Qosa H, Abuasal BS, Romero IA, Weksler B, Couraud PO, Keller JN, et al. Differences in amyloid-beta clearance across mouse and human blood-brain barrier models: kinetic analysis and mechanistic modeling. Neuropharmacology. 2014;79:668–78.
26. Roberts KF, Elbert DL, Kasten TP, Patterson BW, Sigurdson WC, Connors RE, et al. Amyloid-beta efflux from the central nervous system into the plasma. Ann Neurol. 2014;76(6):837–44.
27. Zuroff L, Daley D, Black KL, Koronyo-Hamaoui M. Clearance of cerebral Abeta in Alzheimer's disease: reassessing the role of microglia and monocytes. Cell Mol Life Sci. 2017;74(12):2167–201.
28. Hollingworth P, Harold D, Sims R, Gerrish A, Lambert JC, Carrasquillo MM, et al. Common variants at ABCA7, MS4A6A/MS4A4E, EPHA1, CD33 and CD2AP are associated with Alzheimer's disease. Nat Genet. 2011;43(5):429–35.
29. Naj AC, Jun G, Beecham GW, Wang LS, Vardarajan BN, Buros J, et al. Common variants at MS4A4/MS4A6E, CD2AP, CD33 and EPHA1 are associated with late-onset Alzheimer's disease. Nat Genet. 2011;43(5):436–41.
30. Lambert JC, Heath S, Even G, Campion D, Sleegers K, Hiltunen M, et al. Genome-wide association study identifies variants at CLU and CR1 associated with Alzheimer's disease. Nat Genet. 2009;41(10):1094–9.
31. Guerreiro R, Wojtas A, Bras J, Carrasquillo M, Rogaeva E, Majounie E, et al. TREM2 variants in Alzheimer's disease. N Engl J Med. 2013;368(2):117–27.
32. Jonsson T, Stefansson H, Steinberg S, Jonsdottir I, Jonsson PV, Snaedal J, et al. Variant of TREM2 associated with the risk of Alzheimer's disease. N Engl J Med. 2013;368(2):107–16.
33. Bradshaw EM, Chibnik LB, Keenan BT, Ottoboni L, Raj T, Tang A, et al. CD33 Alzheimer's disease locus: altered monocyte function and amyloid biology. Nat Neurosci. 2013;16(7):848–50.

34. Kleinberger G, Yamanishi Y, Suarez-Calvet M, Czirr E, Lohmann E, Cuyvers E, et al. TREM2 mutations implicated in neurodegeneration impair cell surface transport and phagocytosis. Sci Transl Med. 2014;6(243):243ra86.
35. Gu BJ, Wiley JS. P2X7 as a scavenger receptor for innate phagocytosis in the brain. Br J Pharmacol. 2018;175(22):4195–208.
36. Gu BJ, Duce JA, Valova VA, Wong B, Bush AI, Petrou S, et al. P2X7 receptor-mediated scavenger activity of mononuclear phagocytes toward non-opsonized particles and apoptotic cells is inhibited by serum glycoproteins but remains active in cerebrospinal fluid. J Biol Chem. 2012;287(21):17318–30.
37. Vessey KA, Gu BJ, Jobling AI, Phipps JA, Greferath U, Tran MX, et al. Loss of Function of P2X7 Receptor Scavenger Activity in Aging Mice: A Novel Model for Investigating the Early Pathogenesis of Age-Related Macular Degeneration. Am J Pathol. 2017;187(8):1670–85.
38. Khachiyants N, Trinkle D, Son SJ, Kim KY. Sundown syndrome in persons with dementia: an update. Psychiatry Investig. 2011;8(4):275–87.
39. Gillette-Guyonnet S, Nourhashemi F, Andrieu S, de Glisezinski I, Ousset PJ, Riviere D, et al. Weight loss in Alzheimer disease. Am J Clin Nutr. 2000;71(2):637S-42S.
40. dos Santos VV, Santos DB, Lach G, Rodrigues AL, Farina M, De Lima TC, et al. Neuropeptide Y (NPY) prevents depressive-like behavior, spatial memory deficits and oxidative stress following amyloid-beta (Abeta(1–40)) administration in mice. Behav Brain Res. 2013;244:107–15.
41. Ishii M, Wang G, Racchumi G, Dyke JP, Iadecola C. Transgenic mice overexpressing amyloid precursor protein exhibit early metabolic deficits and a pathologically low leptin state associated with hypothalamic dysfunction in arcuate neuropeptide Y neurons. J Neurosci. 2014;34(27):9096–106.
42. Jeon SG, Hong SB, Nam Y, Tae J, Yoo A, Song EJ, et al. Ghrelin in Alzheimer's disease: Pathologic roles and therapeutic implications. Ageing Res Rev. 2019;55:100945.
43. Duarte-Neves J, Pereira de Almeida L, Cavadas C. Neuropeptide Y (NPY) as a therapeutic target for neurodegenerative diseases. Neurobiol Dis. 2016;95:210–24.
44. Minhas PS, Latif-Hernandez A, McReynolds MR, Durairaj AS, Wang Q, Rubin A, et al. Restoring metabolism of myeloid cells reverses cognitive decline in ageing. Nature. 2021;590(7844):122–8.
45. De la Fuente M, Bernaez I, Del Rio M, Hernanz A. Stimulation of murine peritoneal macrophage functions by neuropeptide Y and peptide YY. Involvement of protein kinase C. Immunology. 1993;80(2):259–65.
46. De la Fuente M, Campos M, Del Rio M, Hernanz A. Inhibition of murine peritoneal macrophage functions by sulfated cholecystokinin octapeptide. Regul Pept. 1995;55(1):47–56.
47. Attwell D, Laughlin SB. An energy budget for signaling in the grey matter of the brain. J Cereb Blood Flow Metab. 2001;21(10):1133–45.
48. Alle H, Roth A, Geiger JR. Energy-efficient action potentials in hippocampal mossy fibers. Science. 2009;325(5946):1405–8.

49. Aldana BI. Microglia-Specific Metabolic Changes in Neurodegeneration. J Mol Biol. 2019;431(9):1830–42.
50. Andersen JV, Christensen SK, Aldana BI, Nissen JD, Tanila H, Waagepetersen HS. Alterations in Cerebral Cortical Glucose and Glutamine Metabolism Precedes Amyloid Plaques in the APPswe/PSEN1dE9 Mouse Model of Alzheimer's Disease. Neurochem Res. 2017;42(6):1589–98.
51. Yin F, Sancheti H, Patil I, Cadenas E. Energy metabolism and inflammation in brain aging and Alzheimer's disease. Free Radic Biol Med. 2016;100:108–22.
52. Nimmerjahn A, Kirchhoff F, Helmchen F. Resting microglial cells are highly dynamic surveillants of brain parenchyma in vivo. Science. 2005;308(5726):1314–8.
53. Yenari MA, Giffard RG. Ischemic vulnerability of primary murine microglial cultures. Neurosci Lett. 2001;298(1):5–8.

# Figures

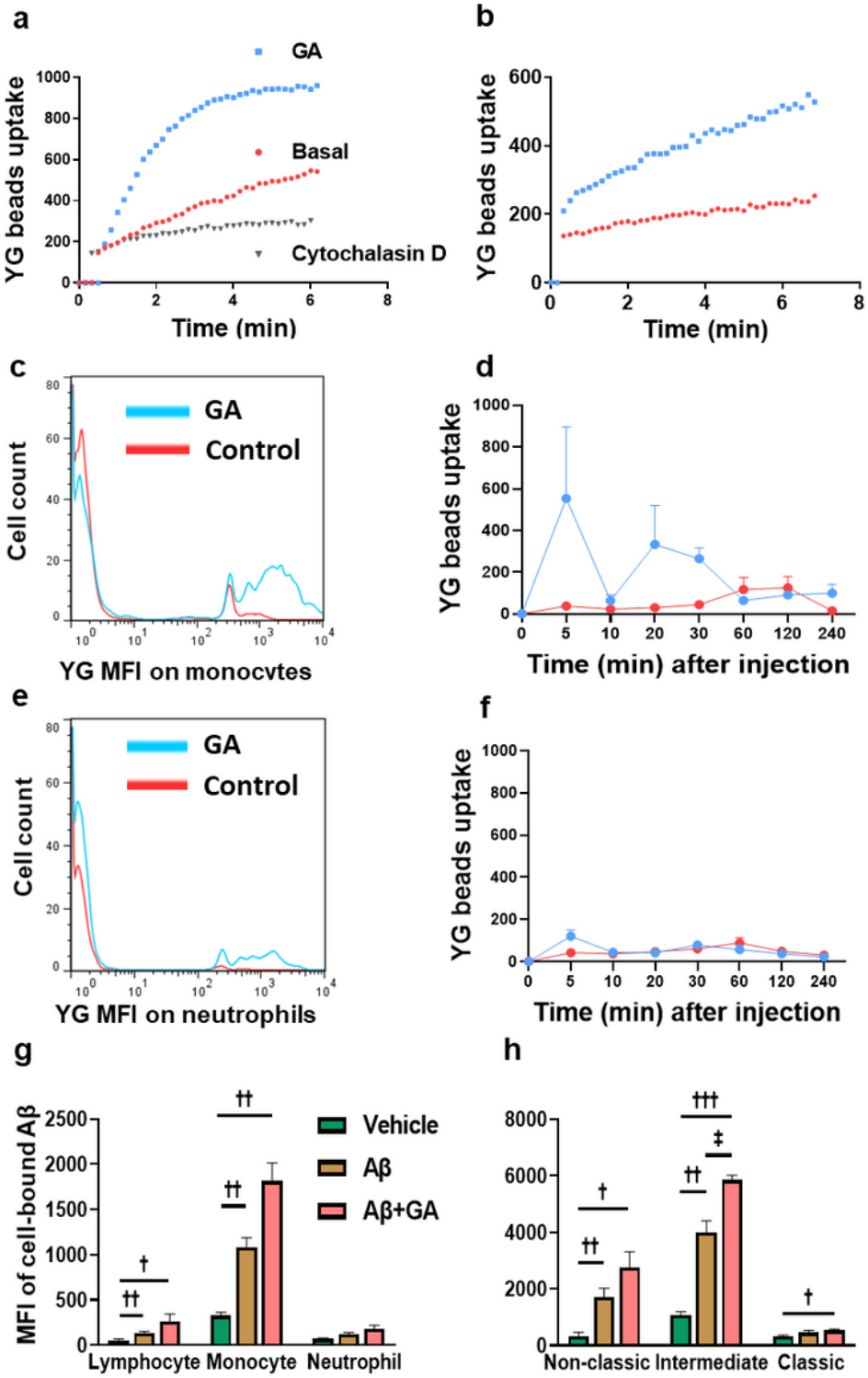


## Figure 1

**GA promotes Aβ recognition and phagocytosis by monocytes in *vitro* and in *vivo*.** The *in vitro* beads uptake was plotted against time by using either human CD14$^+$ monocytes (**a**) or mouse CD11b$^+$ monocytes (**b**). Cells were pretreated with 100 μg/mL GA or without (basal) prior to the addition of YG beads. Results are representative data from multiple individuals. (**c-f**) GA promotes beads uptake by rabbit monocytes (**c&d**) but not neutrophils (**e&f**) *in vivo*. Rabbits were injected intravenously with YG

beads followed by injection of 2 mL/kg GA (n=4) or 4% mannitol (n=3) as control. Beads uptake was measured before injection, and 5-, 10-, 20-, 30-, 60-, 120- and 240-min post injection. **c&e:** YG beads uptake at 30 min after injection. **d&f:** the time course of YG beads uptake. **g**&**h**: *In vitro* Aβ peptide absorption by human leukocytes was checked in the presence and absence of GA. **g&h:** Aβ adhesion to the surface of leukocytes (g) and subgroups of monocytes (h) in the presence (pink) or absence (golden) of GA. The solvent for dissolving Aβ (90% DMSO:10% $H_2O$) is used as the control (green). Results are presented as group means with standard error of the mean (SEM). **†**: significant difference from the vehicle; **‡**: significant difference from the Aβ alone; **†/‡**: 0.01 < P < 0.05; **††**: P < 0.01; **†††**: P < 0.001; and adjusted P was decided by Tukey HSD test.

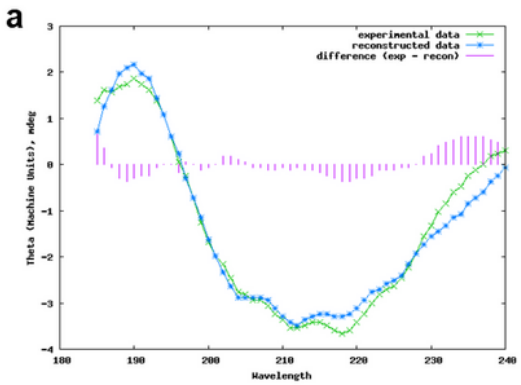


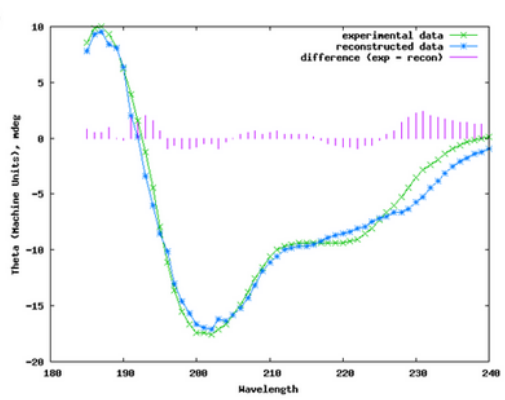


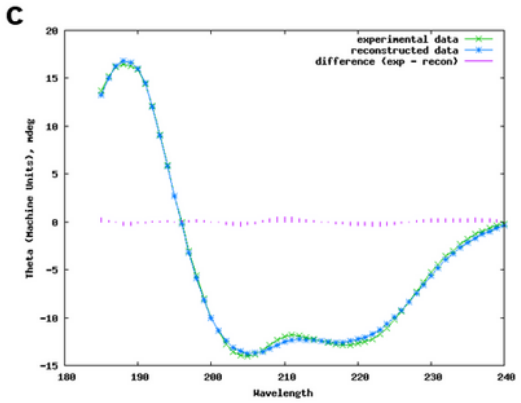


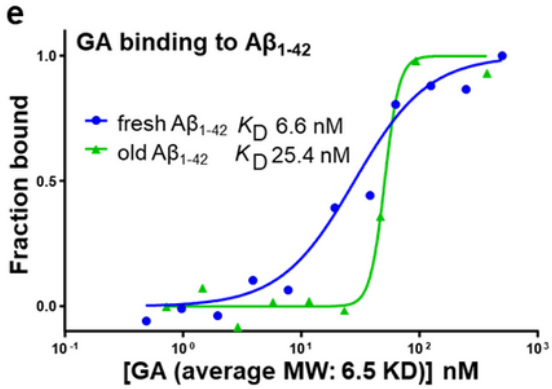


d

| Peptide | Method | α-Helix 1 | α-Helix 2 | β-Strand 1 | β-Strand 2 | Turns | Unordered | Total |
|---|---|---|---|---|---|---|---|---|
| Aβ | CDSSTR* | -0.01 | 0.02 | 0.31 | 0.14 | 0.3 | 0.23 | 1 |
| GA | CDSSTR | -0.01 | 0.01 | 0.18 | 0.1 | 0.3 | 0.45 | 1 |
| Aβ+GA | CDSSTR | 0.04 | 0.05 | 0.26 | 0.13 | 0.2 | 0.33 | 1 |

* Sreerama, N. and Woody, R.W. (2000), Analytical Biochemistry, 287, 252–260 and references therein.

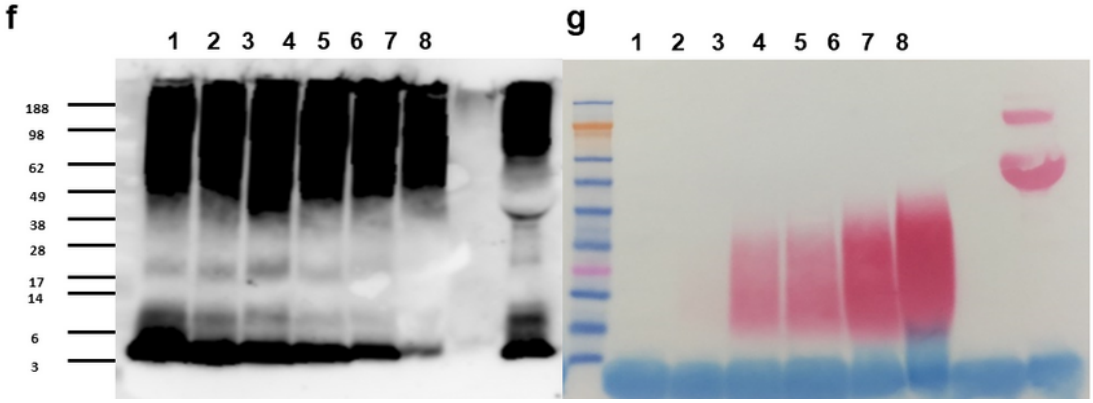


## Figure 2

**GA binds to Aβ with high affinity.** Circular Dichroism spectroscopy (CD) analysis shows secondary structures of Aβ monomer (**a**), GA (**b**) and mixed Aβ and GA(**c**). Fractions were analyzed using CDSSTR method and reference dataset 3 in the article by Sreerama et al was applied (**d**). **e.** HiLyte Fluor488 labelled $Aβ_{1-42}$ (80 nM, in PBS) was mixed 1:1 (volume) with serially diluted GA. Measurements were performed in standard treated capillaries on a Monolith NT.115 system using MicroScale Thermophoresis

(MST) technology. **f**&**g**: Complex of Aβ and GA cannot be separated in reduced SDS-PAGE Western-blotting. $A\beta_{1-42}$ (22 pmol each) was mixed with escalating GA 0, 2.2, 11, 22, 66, 155 pmol (lane 1-6) or bovine serum album (BSA) 22 pmol (lane 8). Lane 7 was blanked. The mixtures (30 µL each) were reduced with 50 µM DTT and heated at 90$^{o}$C for 5 min prior to SDS-PAGE. The proteins were then transferred and probed with the anti-Aβ mAb (clone W0-2). **f.** Immunoblotting image shows Aβ staining. **g.** Ponceau S staining image after proteins were transferred to a nitrocellulose member. GA and BSA in large quantities were stained in the red. The Seeblue Plus 2 pre-stained standard was used to estimate protein size.

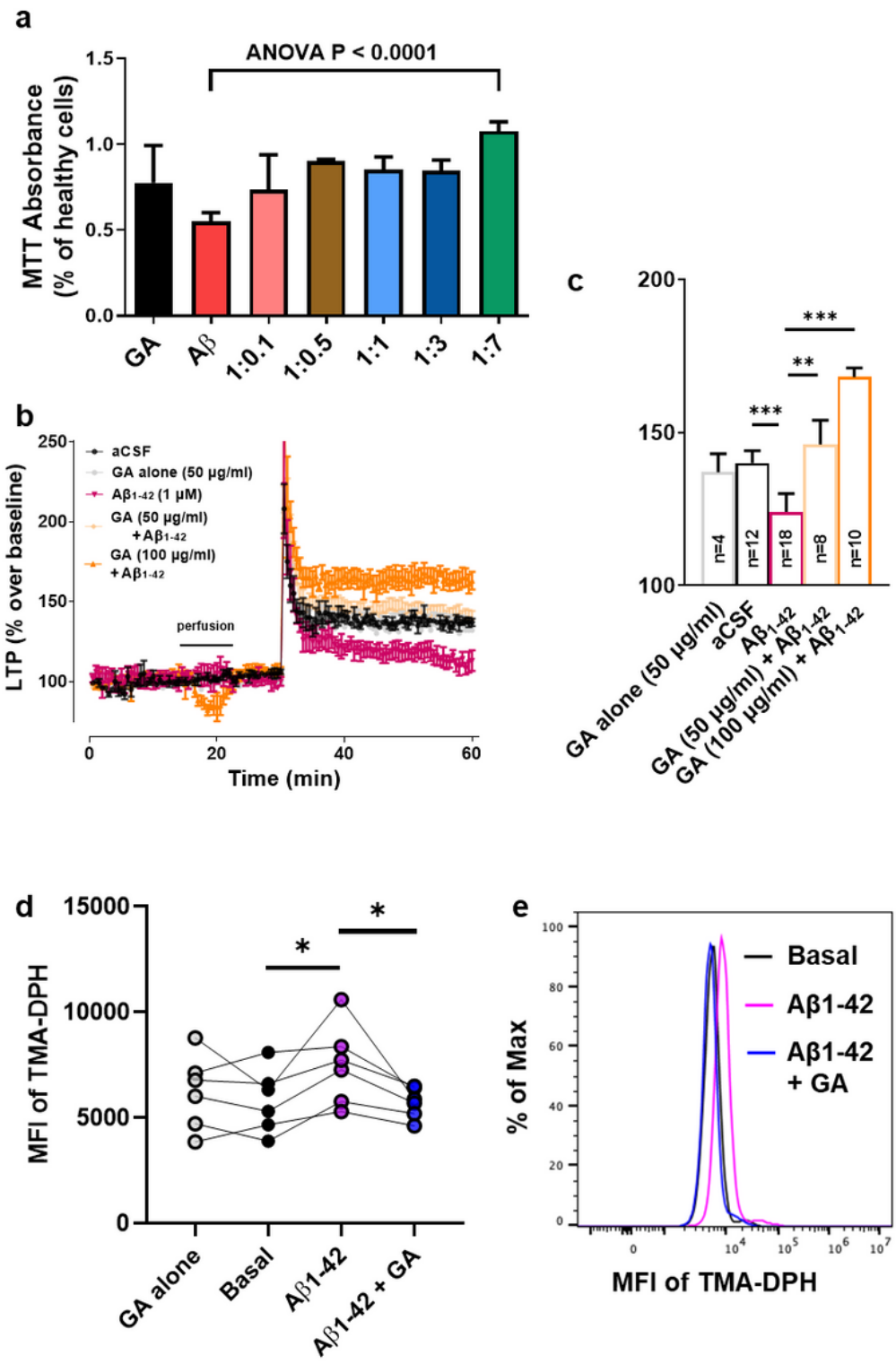


## Figure 3

**GA antagonizes Aβ-induced cytotoxicity *in vitro*. a.** GA rescued cultured neuronal cells from Aβ-induced cytotoxicity. $Aβ_{1-42}$ (final concentration of 10 µM) was mixed with escalating amount of GA by molar ratios: 1:0, 1:0.1, 1:0.5, 1:1, 1:3, 1:7. SH-SY5Y cells were treated with mixtures for 4 hours and were then incubated with MTT substrate for another 4 hours. The absorbance of formazan was measured to estimate cell viability of the treated cells. **b.** GA restored Aβ-induced LTP suppression. 1 µM $Aβ_{1-42}$

(magenta) suppressed hippocampal LTP in comparison to artificial cerebrospinal fluid (aCSF, indigo). 50 μg/ml GA alone had no effect on LTP (purple). The complexing of GA neutralized toxicity of Aβ and restored hippocampal LTP (light green and dark green). Changes (% over baseline) of LTP are shown in a time-course. Statistical data are shown in panel **c. d.** GA antagonized Aβ induced membrane disruption in gated human peripheral blood $CD14^+$ monocytes. A typical graph of functional changes measured by TMA-DPH fluorescent intensity is demonstrated in **e**. Results are presented as group means with standard error of the mean (SEM). *: 0.01 < P < 0.05; **: P < 0.01; ***: P < 0.001.

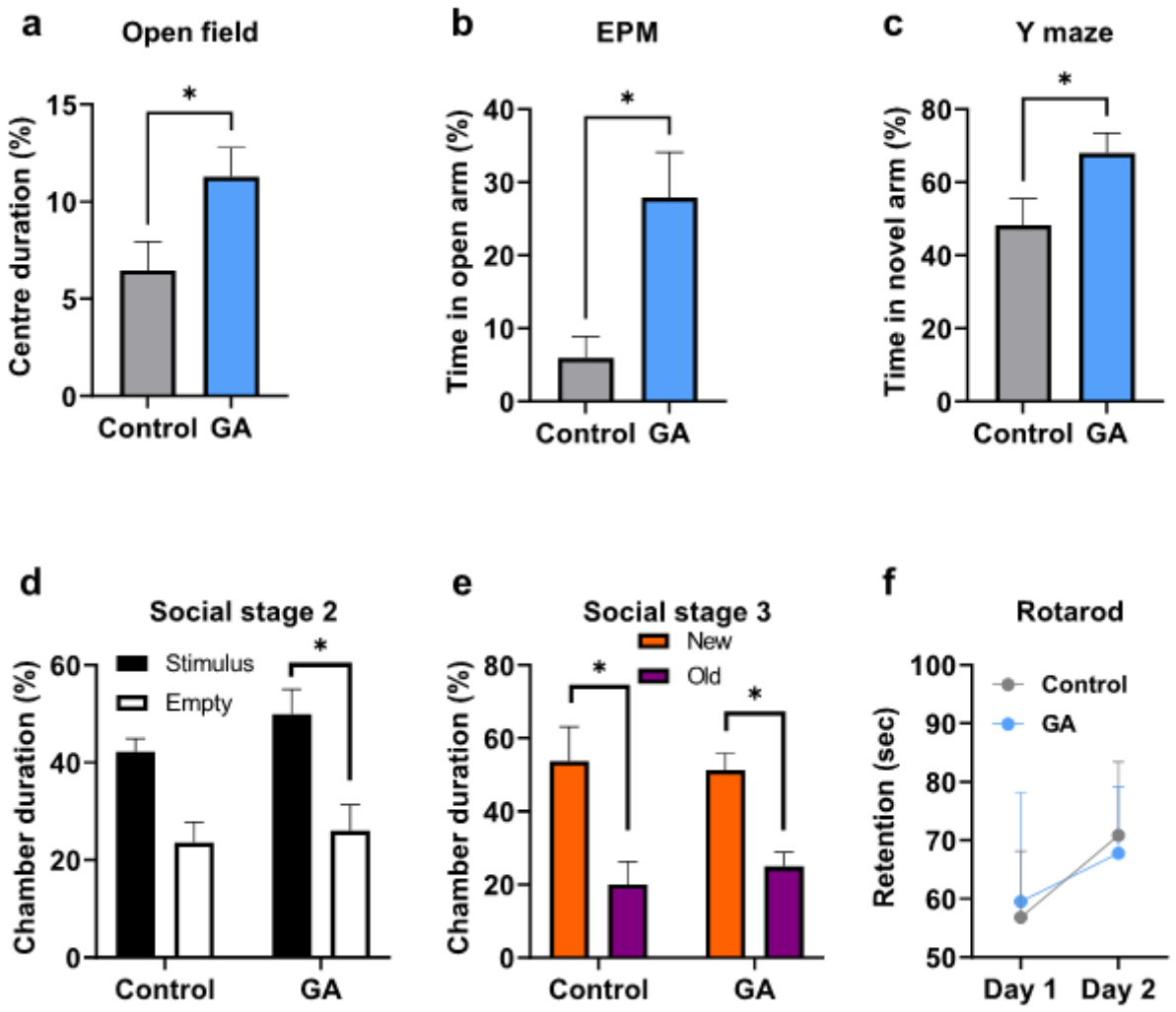


## Figure 4

**GA ameliorates anxiety-like behaviour and improves spatial cognition in an AD mouse model.** Female APP/PS1 mice (21 to 23-month-old) underwent surgery to implant a mini-osmotic pump for intraventricularly delivering GA (n = 10) or the vehicle (saline with 4% mannitol) as control (n = 7). Mice underwent behavioural testing over two consecutive weeks beginning 22 days after implantation. **a.** In the open field test, the percentage score of center duration (%) of GA mice was found significantly higher than controls. **b.** In the elevated plus maze (EPM), the percentage score of the time spent in the open arms (%) of GA was also significantly higher than controls. **c.** In the Y maze, the percentage score of the

time spent in the novel arm (%) was significantly increased in GA compared to controls. **d**. In social interaction stage 2, both GA and controls showed preference to stimulus chamber over empty chamber. No group difference was found. However, GA mice spent significantly longer time in stimulus chamber in a *post hoc* analysis. **e**. In social interaction stage 3, both GA and controls showed preference to the new stimulus chamber over the old stimulus chamber. No group difference was found. **f**. In the rotarod test, no group difference was found. Results are presented as group means with standard error of the mean (SEM). *: 0.01 < P < 0.05.

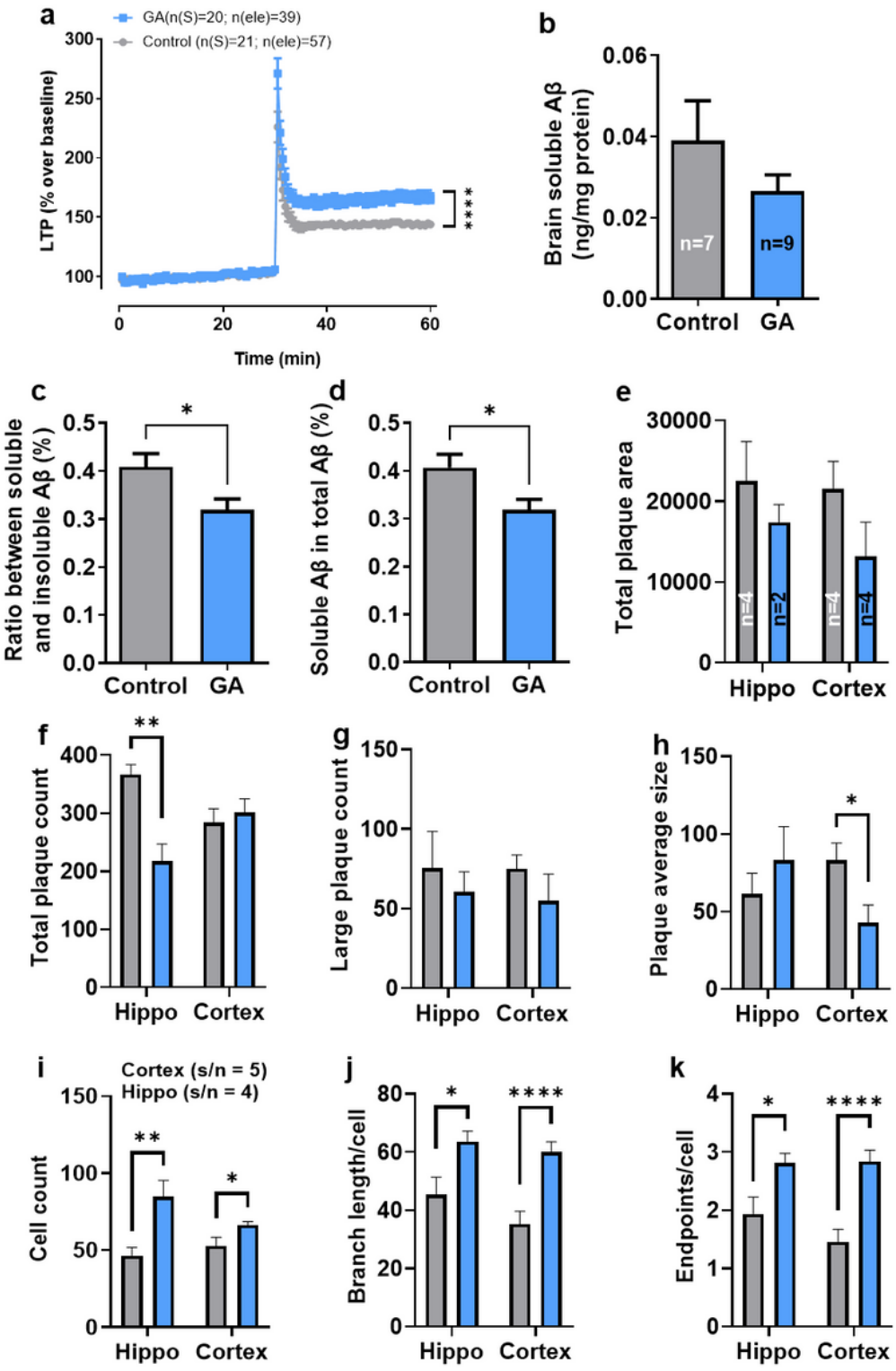

## Figure 5

**GA treated AD mice show signs of functional recovery of neurons and microglia.** Five weeks after mini-osmotic pump implantation, mice were sacrifices and brain were collected. For each mouse, half brain was sliced for LTP assay and immunohistochemical (IHC) staining, and another half was homogenized for Aβ measurement. **a.** LTP assay. The GA group showed significantly improved LTP function compared with controls. n(S): number of slices; n(ele): number of electrodes. **b.** Brain soluble Aβ concentrations as measured by ELISA. The ratio between soluble and insoluble Aβ (%) and the percentage of soluble Aβ in total Aβ (%) are shown in **c&d. e.-h.** IHC staining on brain slices with monoclonal anti-Aβ antibody (clone IE8). Total plaque area (**e.),** all plaque count (**f.),** large plaque count (size > 50 pixels) (**g.)** and plaque average size (**h.)** in both hippocampal and cortical regions are calculated as described in methods and in supplemental Figure 3. Average plaque size is calculated as total plaque area/total plaque count. **i.-k.** IHC staining on brain slices with monoclonal anti-IBA-1 antibody. Microglia activity is evaluated by cell count (**i.**), branch length/cell (**j.**) and endpoints/cell (**k.**). **i.** Results are presented as group means with standard error of the mean (SEM). $^{ns}$: not significant; *: $0.01 < p < 0.05$; **: $p < 0.01$; ****: $p < 0.0001$.

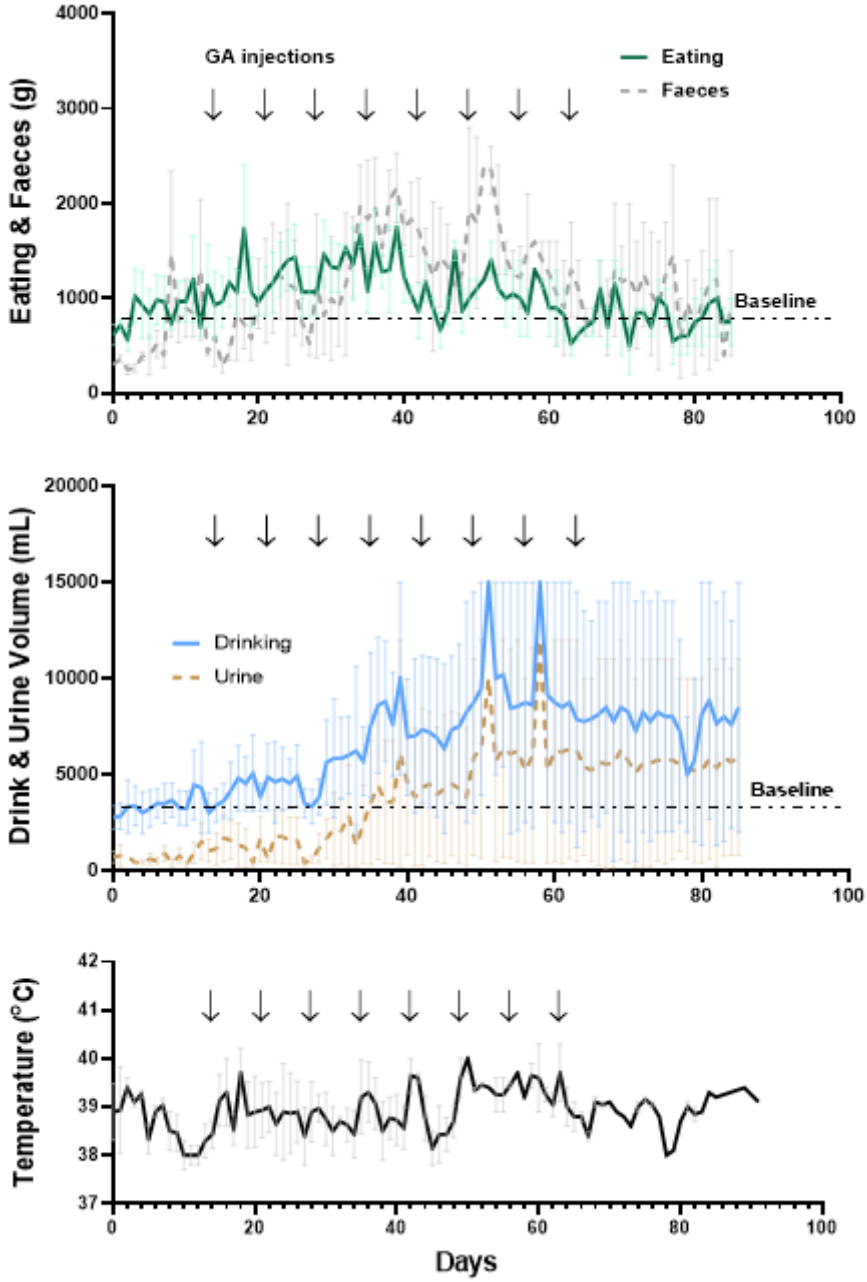


**Figure 6**

**Intraventricular delivery of GA greatly promotes metabolism.** General well-being of sheep was monitored. The sheep underwent ventricular cannulation on the first day and received 8 glatiramer acetate (GA) direct administration via the ventricle (indicated by the arrow) in the following 3 months, 0.5 mL (10 mg) each time. Daily Forage consumption and defecation (top), daily drinking and urinating (middle), anal body temperature (bottom) were monitored. Average eating and drinking before GA treatment were marked as baselines (dash dotted line). Results are presented as group means with standard error of the mean (SEM).

# Supplementary Files

This is a list of supplementary files associated with this preprint. Click to download.

- Graphicabstract05Apr2022.jpg
- SupplementaryInformation.docx